Comparison of Thermal Aging Behavior of CF8 and CF8M Cast Austenitic Stainless Steels

Shoaib Mehboob [a], Hyun Joon Eom [a], Yoohwan Kim[a], Taejeong An[a], Changheui Jang [a*]
[a]*Department of Nuclear and Quantum Engineering, Korea Advanced Institute of Science and Technology, Daejeon, 34141, Republic of Korea*
[*]*Corresponding author: chjang@kaist.ac.kr*

Keywords : thermal aging, embrittlement, stainless steels, kinetics, activation energy

1. Introduction

Cast austenitic stainless steels (CASSs) are widely used for the manufacturing of different primary coolant system components in pressurized water reactors (PWRs). The CASSs possess some amount of δ-ferrite to avoid the hot cracking during solidification of castings. This δ-ferrite undergoes hardening during long-term operations at high temperatures which consequently leads to the loss of fracture toughness of CASS components. The hardening of δ-ferrite is primarily attributed to the spinodal decomposition to Fe-rich (α) and Cr-rich (α′) phases and precipitation of secondary phases (G-phase, ω-phase, etc.). The hardening behavior of δ-ferrite and the embrittlement of CASS is dependent on the composition [1,2].

This study compares the thermal aging behavior of CF8 and CF8M CASSs, with similar ferrite content. The CF8 and CF8M are exposed to thermal aging at 343 °C, 375 °C and 400 °C for up to 15,000 h. The evolution of microstructural features, such as spinodal decomposition, G-phase and ω-phase, with thermal aging is assessed by employing transmission electron microscopy. The degradation of mechanical properties with thermal aging is investigated using Vickers hardness, tensile testing and fracture toughness (J-R) testing. The kinetics of hardening of δ-ferrite and embrittlement of CASSs is assessed by estimating the activation energy using different mechanical properties.

2. Methods and Results

2.1 Experimental

In this study, CF8 and CF8M CASSs manufactured by induction melting and ingot casting were used. The alloys were solution treated at 1150 °C for 2 h followed by water quenching. The composition of alloys measured using inductively coupled plasma (ICP) spectroscopy and δ-ferrite content estimated using phase fraction method are summarized in Table 1. The CF8 and CF8M were subjected to thermal aging at 343 °C, 375 °C and 400 °C for up to 15,000 h, in air.

Table I: Chemical composition (wt. %) and ferrite content of CF8 and CF8M.

	Fe	**Cr**	**Ni**	**Mo**	**Cu**	**C**	**Si**	**Mn**
CF8	Bal.	21.2	8.5	0.2	0.1	0.038	0.9	0.82
CF8M	Bal.	20.3	9.7	2.5	0.1	0.036	0.9	0.86
	Ferrite (Vol. %)							
CF8	21.7							
CF8M	19.6							

The specimens for microstructure analysis were prepared using twin-jet polishing. The microstructure changes in δ-ferrite of CF8 and CF8M were studied using transmission electron microscope. The Vickers hardness was used to analyze the hardness of δ-ferrite in CF8 and CF8M. The tensile testing was performed in accordance with the ASTM E8/E8M-22 [3] and fracture toughness testing was performed in accordance with the ASTM E1820-22 [4] and recommendations by NUREG/CR-4513 [5].

2.2 Microstructure Analysis

The STEM-EDS maps and HRTEM/FFT patterns of δ-ferrite in CF8 and CF8M, after 10,000 h of aging at 400 °C, are shown in Fig. 1. In both CF8 and CF8M, the spinodal decomposition of δ-ferrite to Fe-rich (α) and Cr-rich (α′) phases is observed after thermal aging. The long-term aging also induces the formation of G-phase precipitates in both CF8 and C8M. However, in CF8M, Mo-rich ω-phase precipitates are also observed along with the G-phase precipitates. These ω-phase precipitates are not formed in CF8.

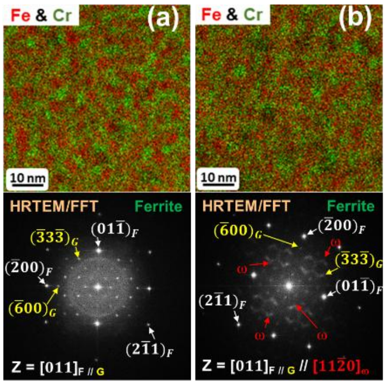

Fig. 1. STEM-EDS (Fe and Cr) maps and HRTEM/FFT patterns of δ-ferrite in (a) CF8 and (b) CF8M, after 10,000 h of aging at 400 °C.

2.3 Mechanical Testing

Fig. 2 (a-c) shows the mechanical properties of CF8 and CF8M, unaged and after thermal aging at 400 °C. It can be seen that there is an increase in strength and loss of fracture toughness for both CF8 and CF8M after thermal aging. Thermal aging induced hardening of δ-ferrite is also observed for both CF8 and CF8M.

Fig. 2 (d) shows the activation energy of thermal aging, estimated using fracture toughness and Vickers hardness of δ-ferrite in CF8 and CF8M. The activation energy measured using fracture toughness (J_{IC} / J_Q and $J_{2.54\ mm}$) indicates faster kinetics of embrittlement for CF8M as compared with the CF8. However, the kinetics of δ-ferrite hardening is relatively faster for CF8 than for CF8M.

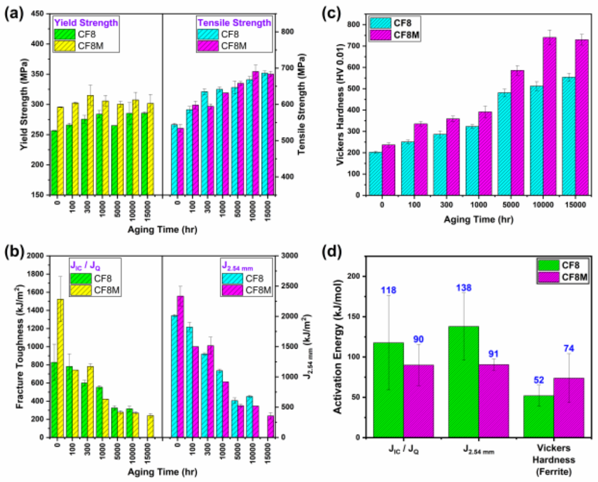

Fig. 2. Mechanical properties of CF8 and CF8M, unaged and aged at 400 °C: (a) yield strength and tensile strength, (b) fracture toughness (J_{IC} / J_Q) and $J_{2.54\ mm}$, (c) Vickers hardness of δ-ferrite. (d) Comparison of activation energies estimated using different mechanical properties of CF8 and CF8M.

3. Conclusions

In this study, the thermal aging behavior of CF8 and CF8M CASS with ~20% of δ-ferrite was compared. The microstructure analysis indicated the spinodal decomposition of δ-ferrite and formation of G-phase in both CF8 and CF8M. In CF8M, precipitates of ω-phase were also formed. The microstructure changes in δ-ferrite led to the hardening of δ-ferrite and consequently loss of fracture toughness for both CF8 and CF8M. The kinetics of thermal aging embrittlement was faster for CF8M as compared to that for CF8.

Acknowledgements

This study was mainly supported by the Nuclear Safety Research Program through the Korea Foundation of Nuclear Safety (KoFONS) using the financial resource granted by the Nuclear Safety and Security Commission (NSSC) of the Republic of Korea. (No. 2103078-0121-SB110 and 1805005-0421-WT112)

REFERENCES

[1] T. G. Lach, T. S. Byun, and K. J. Leonard, "Mechanical property degradation and microstructural evolution of cast austenitic stainless steels under short-term thermal aging," Journal of Nuclear Materials, vol. 497, pp. 139-153, 2017.
[2] S. Mehboob, B. S. Kong, H. J. Eom, and C. Jang, Evolution of nano-sized precipitates in δ-ferrite of high-Cu CF8M with thermal aging and their stability against reversion heat treatment, Journal of Materials Research and Technology (Submitted), 2025.
[3] "ASTM E8/E8M-22, Standard Test Methods for Tension Testing of Metallic Materials," in Annual Book of ASTM Standards, vol. 03.01: ASTM International, 2022.
[4] "ASTM E1820-22, Standard Test Method for Measurement of Fracture Toughness," in Annual Book of ASTM Standards, vol. 03.01: ASTM International, 2022.
[5] O. K. Chopra, Estimation of fracture toughness of cast stainless steels during thermal aging in LWR systems (no. NUREG/CR-4513). Washington, DC: Office of Nuclear Regulatory Research, U.S. Nuclear Regulatory Commission, 2016.